Available online at www.sciencedirect.com
SCIENCE DIRECT
Journal of Sound and Vibration 294 (2006) 454–465
JOURNAL OF SOUND AND VIBRATION
www.elsevier.com/locate/jsvi

Active health monitoring in a rotating cracked shaft using active magnetic bearings as force actuators

G. Mani[a], D.D. Quinn[a,*], M. Kasarda[b]

[a]Department of Mechanical Engineering, The University of Akron, Akron, OH 44325-3903, USA
[b]Department of Mechanical Engineering, Virginia Tech, Blacksburg, VA 24061, USA

Received 30 September 2005; received in revised form 12 October 2005; accepted 4 November 2005
Available online 24 January 2006

Abstract

We consider the active health monitoring of rotordynamic systems in the presence of breathing shaft cracks. The shaft is assumed to be supported by conventional bearings and an active magnetic bearing (AMB) is used in a mid-shaft or outboard location as an actuator to apply specified, time-dependent forcing on the system. These forces, if properly chosen, induce a combination resonance that can be used to identify the magnitude of the time-dependent stiffness arising from the breathing mode of the shaft crack.

1. Introduction

Many critical rotating machines such as compressors, pumps, and gas turbines continue to be used beyond their expected service life despite the associated potential for failure due to damage accumulation. Therefore, the ability to monitor the structural health of these systems is becoming increasingly important, and the term *structural health monitoring* can be defined as the process of implementing a damage-detection strategy. This strategy involves the observation of a structure over a period of time, the identification of features from these measurements, and the analysis of these features to determine the current damage state of the system.

Current monitoring techniques can be loosely classified as either local or non-local in nature. Local methods rely on measurements of the structure near the site of the damage, e.g., visual and ultrasonic methods. As such, the location of the potential damage must be both known a priori and accessible to direct measurement. For non-local techniques the measurement and identification of the system's health is not necessarily correlated with the physical location of the damage. In particular, vibration-based detection methods use the dynamic response of the structure to infer the health of the system [1]. If the accumulated damage alters the dynamic characteristics of the structure (e.g., mass, stiffness, dissipation), the measured response will change accordingly. These changes are often recognized in terms of modal properties [2–4], although recently more advanced techniques have been proposed based on, for example, bifurcations in reduced-order models [5], nonlinear time-series analysis [6,7], and phase space reconstruction [8–10]. In each of these techniques the

*Corresponding author. Tel.: +1 330 972 6302; fax: +1 330 972 6027.
E-mail addresses: gm5@uakron.edu (G. Mani), quinn@uakron.edu (D.D. Quinn), maryk@vt.edu (M. Kasarda).

0022-460X/$ - see front matter © 2006 Elsevier Ltd. All rights reserved.
doi:10.1016/j.jsv.2005.11.020

changes in the observed features are identified with the accumulating level of damage. However, the success of any vibration-based technique is limited by the sensitivity of the response to the accumulated damage [11].

The modeling and dynamical behavior of damaged structures has received substantial attention in the literature (see the reviews by Dimarogonas [12] and Wauer [13]). Plaut and Wauer [14] consider the dynamical behavior of an unbalanced rotating shaft and use the method of multiple scales to identify and analyze several resonances in the system. Chondros and Dimarogonas [15] develop a consistent model for the vibrations of a shaft with an open crack. However, for cracks which periodically open and close in rotating shafts, known as "breathing" cracks, the formulation is much more involved [16]. One simple model, developed by Gasch [17,18], represents the breathing crack as a linear time-varying stiffness in the system.

Traditional methods for the detection of shaft cracks monitor the components of the measured vibration signal that are multiples of the rotational speed under steady-state and transient operation. In addition, the presence of a crack couples the axial, radial, and torsional vibrations of the shaft and several reported works have used this coupling under external excitation as a means to identify the presence of cracks [19,20]. In addition, the spectral components of the shaft response under radial excitation can be used to identify the presence of transverse shaft cracks. In particular, Iwatsubo et al. [21] consider the vibrations of a slowly rotating shaft subject to either periodic or impulsive excitation. They identify specific harmonics in the response spectrum, which are combinations between the rotation speed and excitation frequency, that can be used to detect the presence of the crack. Also, Iwatsubo et al. note that the sensitivity of the response to the magnitude of the damage depends on the value of the excitation frequency chosen for the detection. Finally, Ishida and Inoue [22] consider the response of a horizontal rotor to harmonic external moments. Similar to the present work, they identify forcing frequencies for which the response is sensitive to the presence of the damage. Using the method of harmonic balance, a combination resonance is identified between nonlinear stiffness terms, the operating speed, and the critical speed of the shaft, and the resulting vibration amplitude is proportional to the amplitude of the nonlinearities, which are assumed proportional to the magnitude of the shaft crack.

The majority of applications of AMBs are as active suspension systems for shafts or rotors. Several components of an AMB are characterized by nonlinear behavior and therefore the entire system is inherently nonlinear [23]. In addition to their use as support bearings, AMBs can also be used both as force actuators and sensors [24]. For example, in a rotordynamic system Humphris [25] utilized AMBs for both support and as a means to apply perturbation forces to the shaft, monitoring the response for health diagnosis. Likewise, Kasarda et al. [26] proposed a method utilizing AMBs for the non-destructive evaluation of manufacturing processes. Zhu et al. [27] use the model of Gasch [18] to examine the performance of optimal control methods on the response of a cracked rotor supported by active magnetic bearings (AMBs) and find that the introduction of a breathing crack alters the resulting vibration characteristics of the system and significantly complicates the design and analysis of the AMB controller. However, they note that in certain operating conditions these vibration characteristics can be used to detect the presence of the crack. In the present work, AMBs are used as an actuator for applying multiple types of force inputs to a rotating structure for analysis of the resulting system vibrations. The AMBs are used in conjunction with conventional support bearings, rather than for rotor support, allowing their application to a more general class of rotating machinery than that of purely magnetically supported rotors.

In this paper, the equations of motion for a simple Leval or Jeffcott rotor are first presented, incorporating a breathing crack. These equations, linearized about the static equilibrium position, are then analyzed using the method of multiple scales to identify the resonant operating conditions. In particular, a combination resonance is identified in which the response is sensitive to the magnitude of the accumulating damage, serving as a novel strategy for health monitoring in the system. Furthermore, this proposed damage detection technique does not require the shaft to operate at a specific speed and can therefore be used as an "on-line" health-monitoring strategy under normal loads and steady-state operating conditions. This strategy is verified against numerical simulations of the original equations of motion and even in the presence of noise the response is shown to be sensitive to the magnitude of the damage. The analytical predictions for the response of the damaged system are shown to compare favorably with the numerical results and finally, this serves as an explanation for the sensitivity of the damage detection noted earlier by Iwatsubo et al. [21].

2. Model

2.1. Equations of motion

The equations of motion for a simple rotor with a cracked shaft can be written in a stationary frame of reference as [18,27]:

$$\mathbf{M}\ddot{\mathbf{u}} + \mathbf{C}\dot{\mathbf{u}} + \mathbf{K}(t)\mathbf{u} = \mathbf{f}_g + \mathbf{f}_u + \mathbf{f}_{\mathrm{AMB}}, \tag{1}$$

where

$$\mathbf{M} = \begin{bmatrix} m & 0 \\ 0 & m \end{bmatrix}, \quad \mathbf{C} = \begin{bmatrix} c & 0 \\ 0 & c \end{bmatrix},$$

$$\mathbf{f}_g = \begin{bmatrix} -mg \\ 0 \end{bmatrix}, \quad \mathbf{f}_u = \begin{bmatrix} em\hat{\Omega}^2 \cos(\hat{\Omega}t) \\ em\hat{\Omega}^2 \sin(\hat{\Omega}t) \end{bmatrix}.$$

$\mathbf{f}_g$ represents the gravitational force, $\mathbf{f}_u$ arises from the unbalance, $\mathbf{f}_{\mathrm{AMB}}$ is the external force vector from the AMB, and $\mathbf{K}(t)$ is the time-varying stiffness of the cracked shaft. Finally, as shown in Fig. 1, the displacement of the shaft center is $\mathbf{u}(t)$ and the rotation of the shaft is described by θ, with the shaft assumed to be rotating at constant angular speed $\hat{\Omega}$.

The time dependency of the stiffness matrix is assumed to arise from a "breathing crack" so that $\mathbf{K}(t)$ can be written as

$$\mathbf{K}(t) = \mathbf{K}_0 + \Delta\mathbf{K}(t), \tag{2}$$

where $\mathbf{K}_0$ represents the stiffness matrix of uncracked shaft and $\Delta\mathbf{K}$ is the additive stiffness matrix that describes the change in shaft stiffness with increasing damage, and typically the stiffness degrades with increasing damage [18], although no attempt is made here to relate the crack geometry with changes in stiffness. Instead this work focuses on the changes in the dynamical behavior of the system with variations in the stiffness.

The displacement vector can be decomposed as

$$\mathbf{u}(t) = \mathbf{u}_{\mathrm{eq}} + \mathbf{v}(t), \tag{3}$$

where $\mathbf{u}_{\mathrm{eq}}$ is the deflection of the uncracked rotating shaft due to gravity, such that

$$\mathbf{K}_0\mathbf{u}_{\mathrm{eq}} = \mathbf{f}_g. \tag{4}$$

Here it is assumed that the deflection under the gravitational load is constant in time. Such is the case for an isotropic shaft with stiffness:

$$\mathbf{K}_0 = \begin{bmatrix} k_0 & 0 \\ 0 & k_0 \end{bmatrix} \tag{5}$$

and this form for $\mathbf{K}_0$ is assumed to hold so that $\mathbf{u}_{\mathrm{eq}} = \mathbf{K}_0^{-1}\mathbf{f}_g$.

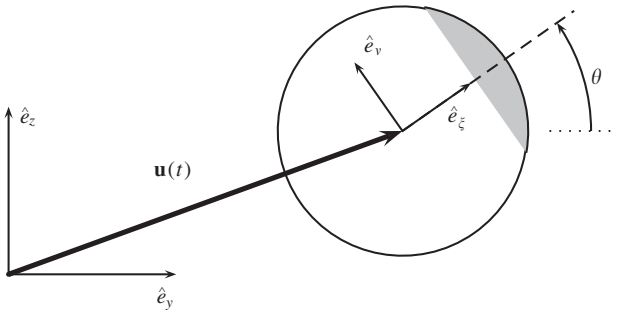

Fig. 1. Cracked shaft model.

In the absence of a rotating imbalance, the equations of motion in terms of $\mathbf{v}$ become

$$\mathbf{M}\ddot{\mathbf{v}} + \mathbf{C}\dot{\mathbf{v}} + (\mathbf{K}_0 + \Delta\mathbf{K}(t))\mathbf{v} = -\Delta\mathbf{K}(t)\mathbf{u}_{\text{eq}} + \mathbf{f}_u + \mathbf{f}_{\text{AMB}}. \tag{6}$$

The above assumes that the small vibrational movement will not affect the additive stiffness matrix provided $|\mathbf{u}_{\text{eq}}| \gg |\mathbf{v}(t)|$, as is the case for a heavy shaft with a large sag and conditions of shaft whirl are precluded from this analysis. With this assumption, the effect of the breathing crack is represented only in the linear time-varying stiffness, although for deeper cracks the nonlinearity of the stiffness plays an important role [12].

2.2. Shaft stiffness

For a breathing crack that opens and closes once per shaft revolution, the additive stiffness matrix $\Delta\mathbf{K}$ is assumed to be time periodic, with period $T = 2\pi/\hat{\Omega}$. Unfortunately, the development of an exact stiffness model of a breathing crack from a fundamental model is quite complicated. Instead, following Gasch [18] the time-varying stiffness is considered directly. In the rotating coordinate system (see Fig. 1), ξ is the coordinate measured in the direction of the crack, v is the cross-crack direction coordinate. Therefore, in this rotating frame of reference $\mathbf{K}$ is considered to be

$$\mathbf{K}_{(\xi,v)}(\theta) = \begin{bmatrix} k_\xi & 0 \\ 0 & k_v \end{bmatrix} = \begin{bmatrix} k_0 - \Delta k_\xi\left(\dfrac{1+\cos(\theta)}{2}\right) & 0 \\ 0 & k_0 - \Delta k_v\left(\dfrac{1+\cos(\theta)}{2}\right) \end{bmatrix}. \tag{7}$$

Here the stiffness is assumed to depend on the rotation of the shaft, where θ is the angle between rotating coordinate system and the reference frame in the ground and recall $\theta(t) = \hat{\Omega}t$. Δk_ξ and Δk_v are the reduction of stiffness at fully open crack in ξ and v directions, respectively. These quantities can be either experimentally determined or empirically related to the crack length and hence the "health" of the shaft. For small cracks (less than the radius of the shaft), Δk_v is small compared to Δk_ξ and can be neglected [18]. With this, the stiffness matrix of the cracked rotor in the stationary coordinate system can be written as

$$\mathbf{K}(\theta) = k_0\begin{bmatrix} 1 & 0 \\ 0 & 1 \end{bmatrix} - \frac{\Delta k_\xi}{4}\begin{bmatrix} f(\theta) & g(\theta) \\ g(\theta) & h(\theta) \end{bmatrix}, \tag{8}$$

where

$$\begin{aligned} f(\theta) &= 1 + \frac{3}{2}\cos(\theta) + \cos(2\theta) + \frac{1}{2}\cos(3\theta) \\ &= \sum_{n=0}^{N} p_n \cos(n\theta), \end{aligned} \tag{9a}$$

$$\begin{aligned} g(\theta) &= \frac{1}{2}\sin(\theta) + \sin(2\theta) + \frac{1}{2}\sin(3\theta) \\ &= \sum_{n=0}^{N} q_n \sin(n\theta), \end{aligned} \tag{9b}$$

$$\begin{aligned} h(\theta) &= 1 + \frac{1}{2}\cos(\theta) - \cos(2\theta) - \frac{1}{2}\cos(3\theta) \\ &= \sum_{n=0}^{N} r_n \cos(n\theta). \end{aligned} \tag{9c}$$

In the absence of damage, the critical frequency of the shaft oscillations is $\sqrt{k_0/m}$, while the opening and closing of the crack, synchronous with the rotational speed $\hat{\Omega}$ of the shaft, introduces a time-varying stiffness.

2.3. Harmonic AMB forcing

The applied AMB forcing is chosen to vary harmonically with frequency $\hat{\Omega}_2$:

$$\mathbf{f}_{\mathrm{AMB}} = \begin{bmatrix} F_{0,z}\cos(\hat{\Omega}_2 t) \\ 0 \end{bmatrix}.$$

Notice that forcing is applied in the z direction only. The coordinates $\mathbf{v}(t) = [z(t)\ \ y(t)]^{\mathrm{T}}$ are scaled by the static displacement $z_{\mathrm{eq}} = mg/k_0$ and time is scaled with the critical frequency, so that $\tau = \sqrt{k_0/m}t$. With these, the non-dimensional equations of motion become

$$\begin{aligned} &\begin{bmatrix} z'' \\ y'' \end{bmatrix} + 2\varepsilon\zeta \begin{bmatrix} z' \\ y' \end{bmatrix} + \begin{bmatrix} z \\ y \end{bmatrix} - \varepsilon\beta \begin{bmatrix} f(\Omega\tau) & g(\Omega\tau) \\ g(\Omega\tau) & h(\Omega\tau) \end{bmatrix} \begin{bmatrix} z \\ y \end{bmatrix} + \varepsilon\alpha \begin{bmatrix} z^3 \\ y^3 \end{bmatrix} \\ &\quad = \gamma \begin{bmatrix} \cos(\Omega_2\tau) \\ 0 \end{bmatrix} + \varepsilon\delta\Omega^2 \begin{bmatrix} \cos(\Omega\tau) \\ \sin(\Omega\tau) \end{bmatrix} + \varepsilon\beta \begin{bmatrix} f(\Omega\tau) \\ g(\Omega\tau) \end{bmatrix} + \begin{bmatrix} w_1(\tau) \\ w_2(\tau) \end{bmatrix} \end{aligned} \tag{10}$$

with

$$\Omega = \frac{\hat{\Omega}}{\sqrt{k_0/m}}, \quad \Omega_2 = \frac{\hat{\Omega}_2}{\sqrt{k_0/m}}, \quad \gamma = \frac{F_{0,z}}{k_0 z_{\mathrm{eq}}},$$
$$\varepsilon\beta = \frac{\Delta k_\xi}{4k_0}, \quad \varepsilon\zeta = \frac{c}{2\sqrt{k_0 m}}, \quad \varepsilon\delta = \frac{e}{z_{\mathrm{eq}}}.$$

In these equations, the quantity ε is simply a non-dimensional scaling parameter used to indicate the relative sizes of the various parameters. The magnitude of the time-varying stiffness is $\varepsilon\beta$. Moreover, β is identified as the "damage" parameter because it represents the magnitude of the stiffness degradation assumed to scale with the damage in the shaft. The AMB forces appear in the model as external excitation, of amplitude γ and frequency Ω_2, and a weak cubic nonlinearity has been added to the stiffness of the system, described by the parameter α. The mass unbalance is proportional to $\varepsilon\delta$ and finally, the terms $w_1(\tau)$ and $w_2(\tau)$ describe noise added to the system representing stochastic forces and unmodeled dynamics. Both stochastic terms are assumed to possess a normal distribution with standard deviation εv.

The resulting mathematical model can be described as two coupled nonlinear equations with both parametric and external excitation. In this model, the critical speed of the shaft has been scaled to unity and the remaining frequencies are relative to this value. In the analysis that follows, a combination resonance is identified between the critical shaft frequency, the shaft rotational speed, and the external frequency of the AMB excitation. The amplitude of the oscillations at this resonant operation is proportional to both the magnitude of the external excitation γ and, more importantly, the magnitude of the shaft damage, described by the non-dimensional quantity $\varepsilon\beta$ in the above equation. Finally, this response is sensitive to changes in Ω_2, the frequency of the AMB excitation. This is expected to provide a means of identifying marginal damage states.

3. Multiple scale analysis

In the absence of noise, with $w_1(\tau) = w_2(\tau) \equiv 0$, multiple scale analysis [28] is applied to analyze the dynamical behavior of Eq. (10). The solution is assumed to take the form $\mathbf{v} = \mathbf{v}_0 + \varepsilon\mathbf{v}_1 + \cdots$ and a slow time scale is explicitly identified as $\eta = \varepsilon\tau$, so that

$$\frac{\mathrm{d}}{\mathrm{d}\tau} = \frac{\partial}{\partial\tau} + \varepsilon\frac{\partial}{\partial\eta}.$$

Substituting these into Eq. (10) and collecting powers of ε, the first-order solution takes the form

$$z_0 = A_1(\eta)\cos(\tau + \omega_1\eta + \phi_1(\eta)) + \Gamma\cos(\Omega_2\tau), \tag{11a}$$

$$y_0 = A_2(\eta)\cos(\tau + \omega_1\eta + \phi_2(\eta)), \tag{11b}$$

where

$$\Gamma = \frac{\gamma}{1-\Omega_2^2}.$$

The quantity Γ reflects, to $\mathcal{O}(1)$, the amplitude of the response at the AMB excitation frequency. In addition, for resonant forcing conditions, listed in Table 1, the response of the system also contains a harmonic component near the critical frequency of the shaft, at $1+\varepsilon\omega_1$. In the method of multiple scales the frequency shift ω_1 and equations governing the slowly varying amplitude and phase, A_i and ϕ_i, respectively, are determined from the $\mathcal{O}(\varepsilon^1)$ equations by requiring that secular terms vanish. This ensures that the approximation given in Eq. (11) is uniform in time.

As listed in Table 1, the internal resonance conditions are satisfied only for specific values of Ω—the AMB forcing does not effect this conditions. However, the operating speed is an independent quantity so that this condition cannot be arbitrarily satisfied. While the external resonance conditions do depend on Ω_2, the predicted responses from the multiple scales analysis are independent of the damage parameter, β. Thus, these conditions cannot be used to characterize the magnitude of β from vibration data. In contrast, the response of the system when operated in a combination resonance condition is sensitive to the magnitude of the damage parameter β. Therefore, this work focuses on the combination resonance as a mechanism for identifying the damage parameter. Specifically, given the operating speed the combination resonance condition can be satisfied with a proper choice of Ω_2 and the resulting amplitude scales linearly with β. The analysis below is focused on the condition $\Omega_2 = \Omega_2^\star \equiv |n\Omega - 1|$ and the response for the remaining condition is analogous.

Upon application of the method of multiple scales near the combination resonance, the resulting slow flow equations in the z direction can be written as

$$\frac{\mathrm{d}A_1}{\mathrm{d}\eta} = \frac{\beta p_n \Gamma}{4}\sin\phi_1 - \zeta A_1, \tag{12a}$$

$$\frac{\mathrm{d}\phi_1}{\mathrm{d}\eta} = \frac{\beta p_n \Gamma}{4A_1}\cos\phi_1 - \sigma_2 + \frac{\beta p_0}{2} + \frac{3\alpha}{4}\left(\frac{A_1^2}{2} + \Gamma^2\right), \tag{12b}$$

where σ_2 is the detuning from the exact resonance, that is $\Omega_2 = \Omega_2^\star + \varepsilon\sigma_2$. This resonance arises from the interaction between the critical speed of the shaft (assumed to be unity in this non-dimensionalization), the AMB frequency Ω_2 and one of the harmonic terms given in Eq. (9a), so that the amplitude of the specific time-dependent stiffness term in resonance (from Eq. (9a)), p_n, appears above. Similar results can be derived for the vibration amplitude in the y direction.

Stationary solutions of the original Eq. (10) correspond to equilibrium points in Eq. (12). From this, the amplitude-detuning relationship is obtained as

$$\frac{\beta p_0}{2} - \sigma_2 + \frac{3\alpha}{4}\left(\frac{A_1^2}{2} + \Gamma^2\right) = \pm\sqrt{\left(\frac{\beta p_n \Gamma}{4A_1}\right)^2 - \zeta^2} \tag{13}$$

Table 1
Resonant forcing conditions

	Resonance condition	Description
1	$\Omega = \frac{1}{3}, \frac{1}{2}, \frac{2}{3}, 1, 2$	Internal
2	$\Omega_2 = 1, 3$	External
3	$\Omega_2 = \lvert n\Omega - 1\rvert, \lvert n\Omega + 1\rvert,\ n = 1, 2, 3$	Combination

and one may also solve for the stationary phase ϕ_1. In the absence of the nonlinearity ($\alpha = 0$), the response amplitude becomes

$$A_1 = \frac{\beta p_n \Gamma}{4\sqrt{\zeta^2 + (\sigma_2 - (\beta p_0/2))^2}}.$$

For $\alpha \neq 0$ the relationship between A_1 and σ_2 cannot be inverted to determine A_1 in terms of σ_2. Instead, Eq. (13) is solved numerically for A_1. Representative results are shown in Fig. 2.

In Fig. 2a, the linear response ($\alpha = 0$) is shown as β varies. As expected, the maximum response increases with increasing β, although the detuning at which the vibration characteristics are most sensitive to the damage also shifts. In Fig. 2b, as the damping ratio ζ increases the amplitude decreases while in Fig. 2c, the response curve bends with increasing magnitude of α, the coefficient of the nonlinearity. This behavior is typical of systems with cubic nonlinearities [28]. However, the maximum amplitude is independent of this coefficient.

From Eq. (13) the maximum amplitude of the response is determined to be

$$A_1^\star = \left(\frac{p_n \Gamma}{4\zeta}\right)\beta, \tag{14}$$

which occurs at a detuning

$$\sigma_2^\star = \frac{\beta p_0}{2} + \frac{3\alpha\Gamma^2}{8}\left(\left(\frac{\beta p_n}{4\zeta}\right)^2 + 2\right). \tag{15}$$

Thus, when the combination resonance is excited the maximum amplitude of the observed vibrations that occur at the critical frequency of the shaft scale linearly with β, the damage parameter, and can be used to

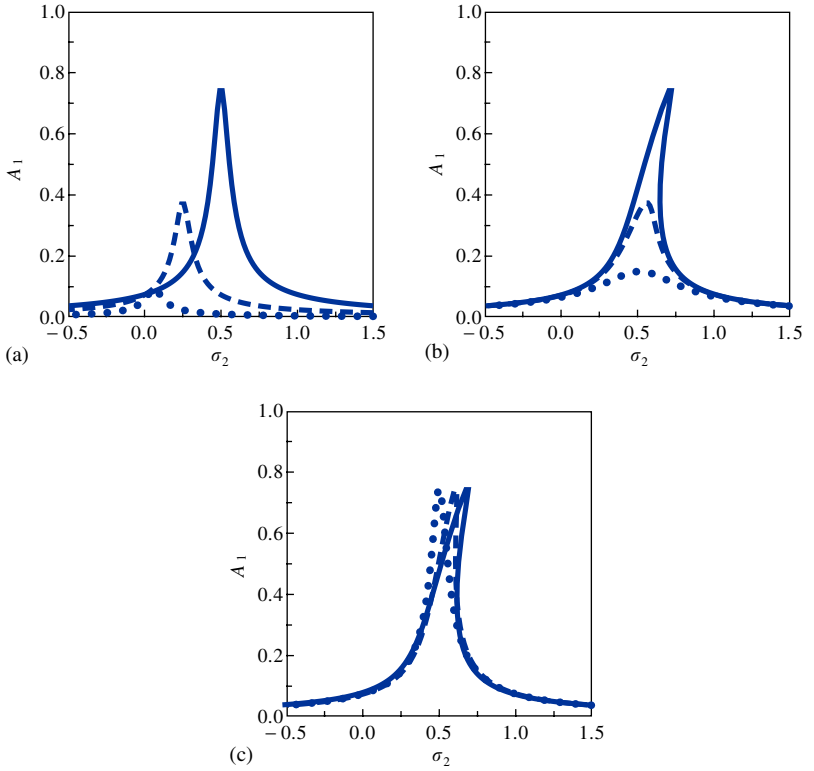

Fig. 2. Damage effect on response amplitude versus detuning curves. Unless otherwise noted, $\beta = 1.00$, $\alpha = 0.25$, $\zeta = 0.05$ ($n = 1$, $\gamma = 1.50$, $\Omega = 5$, $\Omega_2 = 4$): (a) $\beta = (0.125, 0.50, 1.00)$, $\alpha = 0$; (b) $\zeta = (0.05, 0.10, 0.25)$ and (c) $\alpha = (0, 0.50, 1.00)$.

detect and quantify the damage. Notice that the maximum amplitude of the response scales inversely with ζ and is independent of α, the strength of the nonlinearity. Finally, as β increases the detuning at which the maximum response occurs varies as shown in Fig. 3. For $\alpha = 0$ the shift is linear and for non-zero α the detuning varies quadratically with β.

4. Fourier analysis

In Eq. (10), the combination resonance condition is utilized to estimate the shaft damage. From the multiple scales analysis, when the combination resonance condition is satisfied, the amplitude of the response at the critical frequency is predicted to be proportional to β. The results from the multiple scale analysis can be compared against the direct numerical simulation of Eq. (10), obtained using a fourth-order Runge–Kutta algorithm in MATLAB. In the following simulations the stochastic forces are assumed to possess a normal distribution with standard deviation εv.

Fig. 4 depicts two such responses in the z direction for simulations without noise ($v = 0$), while a Fast Fourier Transform (FFT) is used to quantify the response, as shown in Fig. 5. For $\beta \neq 0$ the FFT of the solution in the z direction has two primary peaks: one at the shaft critical frequency and a second at the

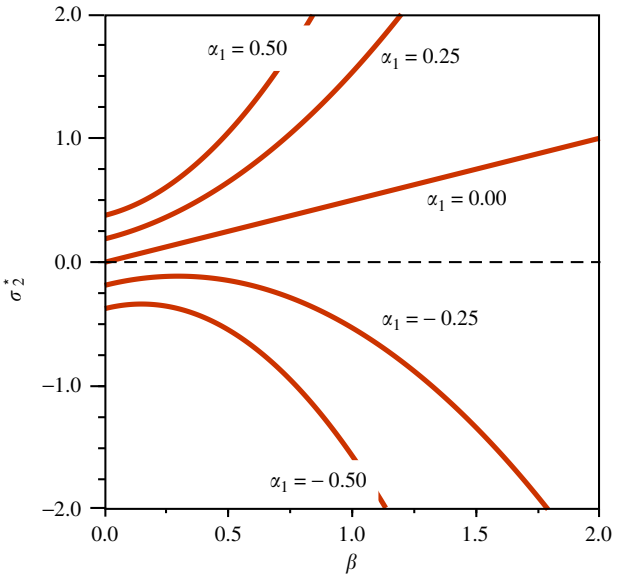

Fig. 3. Shift in the location of the maximum response ($\zeta = 0.10$, $n = 1$, $\Gamma = 1.00$).

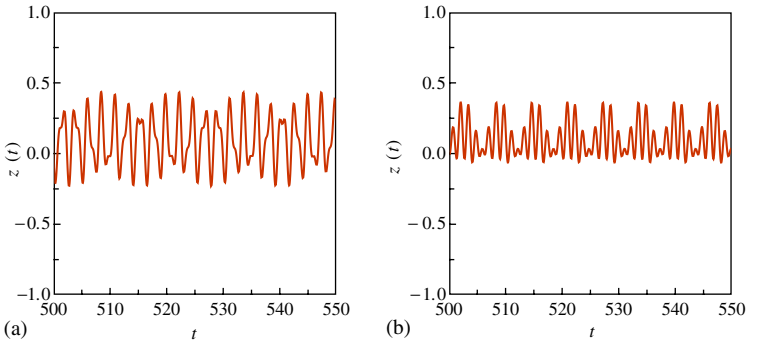

Fig. 4. Numerical integration; $z(t)$ ($\alpha = 0.25$, $\beta = 1.00$, $\gamma = 1.50$, $\zeta = 0.10$, $v = 0$, $\varepsilon = 0.10$, $\Omega = 5$): (a) $\Omega_2 = 2.75$ and (b) $\Omega_2 = 4.00$.

external excitation frequency from the AMBs. Recall that the external forcing is applied only in the z direction. The following analysis focuses on the response in the z direction as a basis for damage detection.

As illustrated in Figs. 4 and 5, the amplitude at the critical frequency (unity in this non-dimensionalization) is considerably larger when the AMB forces occur at the combination resonant frequency ($\Omega_2 = |5 - 1| = 4$) than when the AMB is driven at an arbitrary frequency (e.g., $\Omega_2 = 2.75$) away from the resonant frequency. It is noted that both Ω and Ω_2 are chosen away from both the internal and external resonances (see Table 1).

In the damaged system a peak will occur near the critical frequency, whose amplitude depends on the magnitude of the damage parameter β. As illustrated in Fig. 6, three excitation frequencies are chosen near the

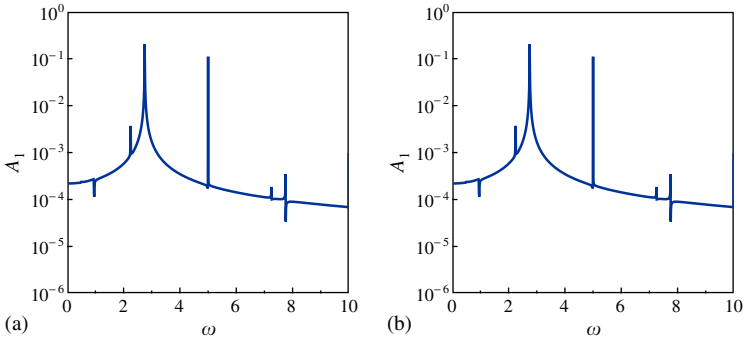

Fig. 5. Comparison of the FFT amplitudes at resonant and non-resonant forcing frequencies ($\alpha = 0.25$, $\beta = 1.00$, $\gamma = 1.50$, $\zeta = 0.10$, $v = 0$, $\varepsilon = 0.10$, $\Omega = 5$). The non-resonant response, with $\Omega_2 = 2.75$, is shown as the solid line, while the resonant response, $\Omega_2 = 4$ is dashed: (a) non-resonant; $\Omega_2 = 2.75$ and (b) resonant; $\Omega_2 = 4.00$.

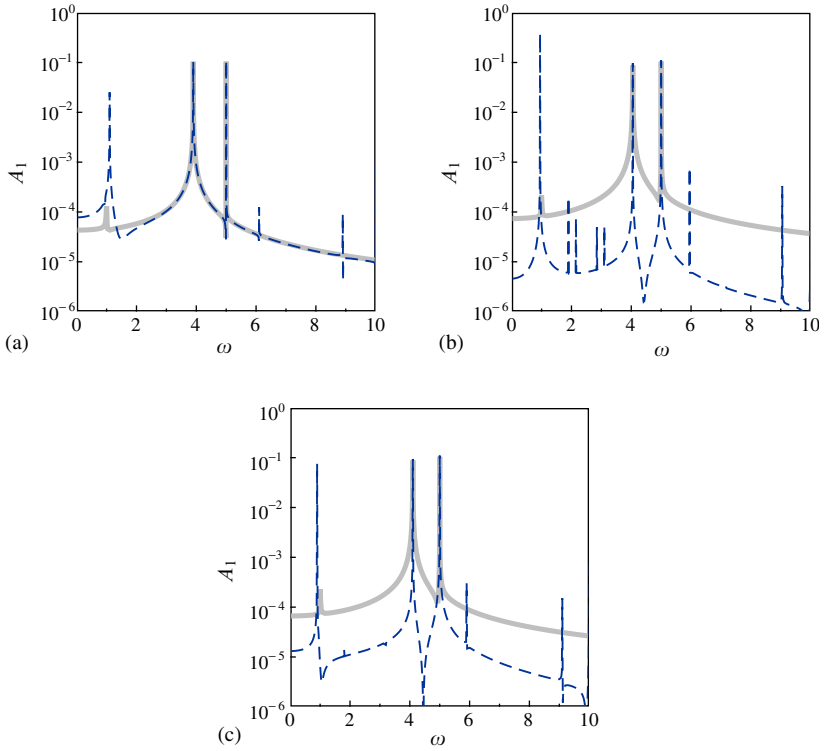

Fig. 6. Comparison of FFT amplitudes below, at and above resonant forcing frequencies for both undamaged and damaged systems ($\alpha = 0.25$, $\gamma = 1.50$, $\zeta = 0.10$, $\varepsilon = 0.10$, $\Omega = 5$). Solid and dashed lines represent undamaged ($\beta = 0$) and damaged ($\beta = 1.00$) systems, respectively: (a) $\sigma_2 = -1.00$, (b) $\sigma_2 = 0.50$ and (c) $\sigma_2 = 1.00$.

combination resonance: $\sigma_2 = -1.00$ (below resonance), $\sigma_2 = 0.50$ (resonance), and $\sigma_2 = 1.00$ (above resonance). The amplitude of the external AMB forcing γ remains constant between these cases and the response of the undamaged system is relatively insensitive to variations in the external forcing frequency. In contrast to the undamaged system ($\beta = 0$), the damaged systems show a peak at the critical frequency and as expected from the multiple scale analysis, the amplitude of this component depends on the detuning from the combination resonance.

Therefore, as the external AMB forcing frequency varies near the combination resonance, the magnitude of the response at the critical frequency varies as well. In Fig. 7a, the maximum amplitude near the critical frequency is shown as the AMB detuning varies. Each curve corresponds to a different value of β, the damage parameter. Clearly, as the damage increases the amplitude of the response increases as well, accompanied by a shift in the value of detuning at which the maximum occurs. These results, obtained from the original equations, can be compared to the results from the multiple scales analysis shown in Fig. 7b. When the system is excited away from the resonant frequency, the sensitivity of the response to the damage is negligible—the response near the critical frequency is small. Only when the system is driven near the resonant forcing is the amplitude of the response comparable to (or larger than) the component of the response at the AMB forcing frequency.

Finally, as β increases the amplitude of the response at the critical frequency increases as well. From the multiple scales analysis, this amplitude is expected to increase linearly in β (see Eq. (14)), which is verified from

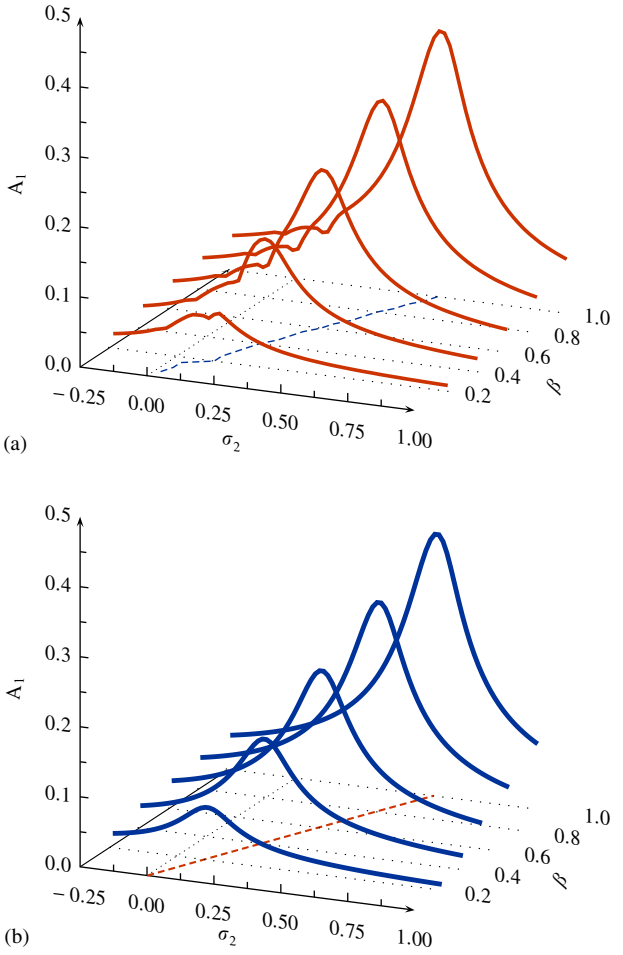

Fig. 7. Damaged FFT amplitude in the vicinity of the resonant forcing frequency ($\alpha = 0.25$, $\gamma = 1.50$, $\zeta = 0.10$, $\Omega = 5$). The dashed curve projected onto the horizontal plane shows the location of the maximum response: (a) numerical results and (b) analytical results.

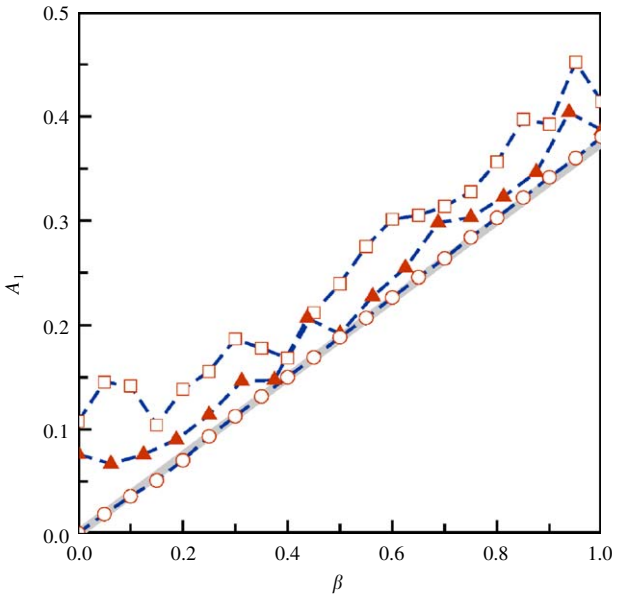

Fig. 8. Maximum response amplitude with increasing damage ($\alpha = 0.25$, $\gamma = 1.50$, $\zeta = 0.10$, $\Omega = 5$); circles: $v = 0$; triangles: $v = 0.50$; squares: $v = 1.00$.

the Fourier analysis of the original equations. In Fig. 8 the amplitude at the critical frequency is shown as a function of β, for three different noise levels, as measured by their standard deviation εv. In the absence of noise for $v = 0$, shown with open circles, the amplitude of the response at the fundamental frequency increases almost linearly with increasing β. This amplitude, obtained from numerical simulations of Eq. (10), is almost coincident with predictions from the multiple scales analysis, from Eq. (14), shown with the solid light gray line. As the magnitude of the noise increases, for sufficiently large damage the amplitude continues to increase with increasing β. However, for low values of β the response of the system is lost within the underlying response due to the noise.

5. Discussion and conclusions

The current work investigates the vibrational response of a cracked rotating shaft subject to applied forces from AMBs. The analysis is based on a phenomenological model, developed originally by Gasch [17], which incorporates the breathing of the crack, nonlinear shaft bending stiffness, and the external forces from the AMBs. Through the method of multiple scales a combination resonance is identified between the critical frequency of the shaft, the operating speed of the shaft, and the frequency of the AMB excitation. Therefore, because the excitation frequency can be chosen arbitrarily, this resonance condition can be satisfied for any combination of critical shaft frequency and operating speed. Moreover, when this resonance occurs the spectral analysis of the damaged shaft vibration response contains a component at the critical frequency (in addition to a component at the excitation frequency). The amplitude of this component at the critical frequency is proportional to the magnitude of the time-dependent stiffness introduced by the breathing crack. Therefore, this relationship provides a mechanism to detect and quantify the presence of breathing cracks in rotating shafts subject to harmonic forcing applied by AMBs. Current efforts are directed toward experimental verification of this work and the application of more advanced damage detection techniques.

Acknowledgments

This material is based upon work supported by the National Science Foundation under Grant No. CMS-0219701. Any opinions, findings, and conclusions or recommendations expressed in this material are those of

the authors and do not necessarily reflect the views of the National Science Foundation. The authors would like to thank Dr. Jonathan Nichols of the US Naval Research Laboratory for helpful discussions and review of an earlier draft.

References

[1] C.R. Farrar, S.W. Doebling, D.A. Nix, Vibration-based structural damage identification, *Proceedings of the Royal Society of London Series A* 359 (2001) 131–149.
[2] D. Capecchi, F. Vestroni, Monitoring of structural systems by using frequency data, *Earthquake Engineering and Structural Dynamics* 28 (1999) 447–461.
[3] Y.-S. Lee, M.-J. Chung, A study on crack detection using eigenfrequency test data, *Computers and Structures* 77 (3) (2000) 327–342.
[4] B.P. Nandwana, S.K. Maiti, Detection of the location and size of a crack in stepped cantilever beams based on measurements of natural frequencies, *Journal of Sound and Vibration* 203 (3) (1997) 435–446.
[5] D.E. Adams, M. Nataraju, A nonlinear dynamical systems framework for structural diagnosis and prognosis, *International Journal of Engineering Science* 40 (2002) 1919–1941.
[6] J.M. Nichols, M.D. Todd, M. Seaver, L.N. Virgin, Use of chaotic excitation and attractor property analysis in structural health monitoring, *Physical Review E* 67 (1) (2003) 016209.
[7] J.M. Nichols, S.T. Trickey, M.D. Todd, L.N. Virgin, Structural health monitoring through chaotic interrogation, *Mechanica* 38 (2003) 239–250.
[8] D. Chelidze, J.P. Cusumano, A dynamical systems approach to failure prognosis, *Journal of Vibration and Acoustics* 126 (1) (2004) 2–8.
[9] D. Chelidze, J.P. Cusumano, A. Chatterjee, A dynamical systems approach to damage evolution tracking, part 1: description and experimental application, *Journal of Vibration and Acoustics* 124 (2) (2002) 250–257.
[10] J.P. Cusumano, D. Chelidze, A. Chatterjee, A dynamical systems approach to damage evolution tracking, part 2: model-based validation and physical interpretation, *Journal of Vibration and Acoustics* 124 (2) (2002) 258–264.
[11] M.D. Todd, J.M. Nichols, C.J. Nichols, L.N. Virgin, An assessment of modal property effectiveness in detecting bolted joint degradation: theory and experiment, *Journal of Sound and Vibration* 275 (2004) 1113–1126.
[12] A.D. Dimarogonas, Vibration of cracked structures: a state of the art review, *Engineering Fracture Mechanics* 55 (5) (1996) 831–857.
[13] J. Wauer, Dynamics of cracked rotors: a literature review, *Applied Mechanics Reviews* 43 (1) (1990) 13–18.
[14] R.H. Plaut, J. Wauer, Parametric, external, and combination resonances in coupled flexural and torsional oscillations of an unbalanced rotating shaft, *Journal of Sound and Vibration* 183 (5) (1995) 889–897.
[15] T.G. Chondros, A.D. Dimarogonas, A consistent cracked bar vibration theory, *Journal of Sound and Vibration* 200 (3) (1997) 303–313.
[16] J. Wauer, Modelling and formulation of equations of motion for cracked rotating shafts, *International Journal of Solids and Structures* 26 (8) (1990) 901–914.
[17] R. Gasch, Dynamic behavior of a simple rotor with a cross-sectional crack, in: *Vibrations in Rotating Machinery*, The Institution of Mechanical Engineers, 1976, Paper C178/76, pp. 123–128.
[18] R. Gasch, A survey of the dynamic behavior of a simple rotating shaft with a transverse crack, *Journal of Sound and Vibration* 160 (2) (1993) 313–332.
[19] K.R. Collins, R.H. Plaut, J. Wauer, Detection of cracks in rotating Timoshenko beams using axial impluses, *Journal of Vibration and Acoustics* 113 (1991) 74–78.
[20] A.K. Darpe, K. Gupta, A. Chawla, Coupled bending, longitudinal and torsional vibrations of a cracked rotor, *Journal of Sound and Vibration* 269 (2004) 33–60.
[21] T. Iwatsubo, S. Arii, A. Oks, Detection of a transverse crack in a rotor shaft by adding external force, in: *Proceedings of the International Conference on Vibrations in Rotating Machinery*, no. C432/093, IMechE, 1992, pp. 275–282.
[22] Y. Ishida, T. Inoue, Detection of a rotor crack by a periodic excitation, in: *Proceedings of ISCORMA*, 2001, pp. 1004–1011.
[23] J.C. Ji, C.H. Hansen, Nonlinear oscillations of a rotor in active magnetic bearings, *Journal of Sound and Vibration* 240 (4) (2001) 599–612.
[24] J. Marshall, M. Kasarda, J. Imlach, A multi-point measurement technique for the enhancement of force measurement with active magnetic bearings, IGTI/TURBO EXPO, New Orleans, LA, 2001 (2001-GT-0246).
[25] R.R. Humphris, A device for generating diagnostic information for rotating machinery using magnetic bearings, in: *Proceedings of the Magnetic Bearings, Magnetic Drives, and Dry Gas Seals Conference and Exhibition*, Alexandria, VA, 1992, pp. 123–135.
[26] M. Kasarda, J. Imlach, P.A. Balaji, The concurrent use of magnetic bearings for rotor support and force sensing for the nondestructive evaluation of manufacturing processes, in: *SPI Seventh International Symposium on Smart Structures and Materials*, Newport Beach, CA, 2000.
[27] C. Zhu, D.A. Robb, D.J. Ewins, The dynamics of a cracked rotor with an active magnetic bearing, *Journal of Sound and Vibration* 265 (3) (2003) 469–487.
[28] A.H. Nayfeh, D.T. Mook, *Nonlinear Oscillations*, Wiley, New York, 1979.